



# Prolonged Mek1/2 suppression impairs the developmental potential of embryonic stem cells

## Citation

Choi, Jiho, Aaron J. Huebner, Kendell Clement, Ryan M. Walsh, Andrej Savol, Kaixuan Lin, Hongcang Gu, et al. 2017. "Prolonged Mek1/2 Suppression Impairs the Developmental Potential of Embryonic Stem Cells." *Nature* (July 26). doi:10.1038/nature23274.

## Published Version

doi:10.1038/nature23274

## Permanent link

<http://nrs.harvard.edu/urn-3:HUL.InstRepos:34361426>

## Terms of Use

This article was downloaded from Harvard University's DASH repository, and is made available under the terms and conditions applicable to Other Posted Material, as set forth at <http://nrs.harvard.edu/urn-3:HUL.InstRepos:dash.current.terms-of-use#LAA>

## Share Your Story

The Harvard community has made this article openly available.  
Please share how this access benefits you. [Submit a story](#).

[Accessibility](#)

1 **Prolonged Mek1/2 suppression impairs the developmental potential of**  
2 **embryonic stem cells**

3  
4  
5 Jiho Choi<sup>1-4,\*</sup>, Aaron J Huebner<sup>1-4,\*</sup>, Kendell Clement<sup>3-5</sup>, Ryan M Walsh<sup>1-4</sup>, Andrej  
6 Savol<sup>1</sup>, Kaixuan Lin<sup>6</sup>, Hongcang Gu<sup>5</sup>, Bruno Di Stefano<sup>1-4</sup>, Justin Brumbaugh<sup>1-4</sup>,  
7 Sang-Yong Kim<sup>7</sup>, Jafar Sharif<sup>8</sup>, Christopher M. Rose<sup>9</sup>, Arman Mohammad<sup>5</sup>,  
8 Junko Odajima<sup>2</sup>, Jean Charron<sup>10</sup>, Toshi Shioda<sup>2</sup>, Andreas Gnirke<sup>5</sup>, Steven Gygi<sup>9</sup>,  
9 Haruhiko Koseki<sup>8</sup>, Ruslan I. Sadreyev<sup>1</sup>, Andrew Xiao<sup>6</sup>, Alexander Meissner<sup>3-5</sup>,  
10 Konrad Hochedlinger<sup>1-4,#</sup>

11  
12  
13  
14 <sup>1</sup> Massachusetts General Hospital Department of Molecular Biology, Boston,  
15 MA 02114, USA

16  
17 <sup>2</sup> Massachusetts General Hospital Cancer Center and Center for Regenerative  
18 Medicine, Boston, MA 02114, USA

19  
20 <sup>3</sup> Department of Stem Cell and Regenerative Biology, Harvard University,  
21 Cambridge, MA 02138, USA

22  
23 <sup>4</sup> Harvard Stem Cell Institute, 1350 Massachusetts Avenue, Cambridge, MA  
24 02138, USA

25  
26 <sup>5</sup> Broad Institute of MIT and Harvard, Cambridge, MA 02142, USA

27  
28 <sup>6</sup> Department of Genetics, Yale University School of Medicine, 10 Amistad  
29 Street, New Haven, CT 06519, USA

30  
31 <sup>7</sup> New York University Langone Medical Center, New York, NA 10016, USA

32  
33 <sup>8</sup> Center for Integrative Medical Sciences, RIKEN National Research and  
34 Development Agency, 1-7-22 Suehiuro-cho, Tsurumi-ku, Yokohama-shi,  
35 Kanagawa-ken, Japan 230-0045

36  
37 <sup>9</sup> Department of Cell Biology, Harvard Medical School, 240 Longwood Avenue,  
38 Boston, MA 02115, USA

39  
40 <sup>10</sup> Centre de recherche sur le cancer de l'Université Laval, CRCHU de Québec,  
41 L'Hôtel-Dieu de Québec, 9, rue McMahan, Quebec, QC, Canada, G1R 2J6

47 \* Co-first authors  
48 # Corresponding author ([khochedlinger@mgh.harvard.edu](mailto:khochedlinger@mgh.harvard.edu))  
49

50 **Concomitant activation of the Wnt pathway and suppression of Mapk**  
51 **signaling by two small molecules in the presence of LIF (2i/L) induces a**  
52 **naïve state in mouse embryonic stem cells (ESCs) that resembles the inner**  
53 **cell mass (ICM) of the pre-implantation embryo<sup>1</sup>. Since the ICM exists only**  
54 **transiently *in vivo*, it remains unclear how sustained propagation of naïve**  
55 **ESCs *in vitro* affects their stability and functionality. Here we show that**  
56 **prolonged culture of male ESCs in 2i/L results in irreversible epigenetic**  
57 **and genomic changes that impair their developmental potential.**  
58 **Additionally, we find that female ESCs cultured in conventional serum/LIF**  
59 **(S/L) media phenocopy male ESCs cultured in 2i/L. Mechanistically, we**  
60 **demonstrate that Mek1/2 inhibition is predominantly responsible for these**  
61 **effects, in part through downregulation of DNA methyltransferases and**  
62 **their associated cofactors. Finally, we show that replacement of the Mek1/2**  
63 **inhibitor with a Src inhibitor preserves the epigenetic and genomic integrity**  
64 **as well as developmental potential of ESCs. Taken together, our data**  
65 **suggest that, while short-term suppression of Mek1/2 in ESCs helps**  
66 **maintain an ICM-like epigenetic state, prolonged suppression results in**  
67 **irreversible changes that compromise their developmental potential.**

68 Dysregulation of Wnt/Mapk signaling as well as DNA methylation have  
69 been linked to cellular transformation and chromosomal instability in ESCs<sup>2-5</sup>.  
70 Therefore, we sought to determine whether sustained perturbation of the  
71 Mapk/Wnt pathway and associated DNA hypomethylation during 2i/L culture  
72 impacts the stability and functionality of ESCs. Specifically, we utilized three  
73 isogenic male ESC lines (129S6 x C57B6 F1) that were derived in 2i/L and then  
74 cultured in S/L for 4 additional passages (p) (Fig. 1a). Each ESC line was  
75 subsequently passaged onto a feeder layer of irradiated MEFs in either 2i/L or  
76 S/L and propagated for an additional 6 or 16 passages (final p10 or p20,  
77 respectively). To assess the reversibility of any observed changes, we also  
78 switched the p20 2i/L-cultured ESC lines back into S/L for an additional 3 or 10  
79 passages.

80 We assessed global DNA methylation patterns in our cultured ESCs using  
81 reduced representation bisulfite sequencing (RRBS). Similar to previous reports<sup>6-</sup>  
82 <sup>8</sup>, global methylation levels of 2i/L-cultured ESCs were lower than S/L-cultured  
83 ESCs and became remethylated when switched back to S/L (Extended Data Fig.  
84 1a-c). This demethylation and subsequent remethylation occurs across most  
85 methylated features including CpG islands, shores, SINEs, LINEs and LTRs  
86 (Extended Data Fig. 1d,e). In contrast, 2i/L culture caused a progressive and  
87 irreversible erosion of DNA methylation at the majority of imprinted control  
88 regions (ICRs), resulting in the biallelic expression of the imprinted gene, *Impact*  
89 (Fig. 1b-d and Extended Data Fig. 1f,g). Additionally, we confirmed biallelic  
90 expression of additional imprinted genes using a *Mus musculus* x *Mus spretus*  
91 F1 stem cell line cultured in 2i/L for 6 passages (Extended data Fig. 1h).

92 Considering that genomic imprinting is essential for development, these results  
93 suggest that 2i/L-cultured ESCs may

94 Female ESCs cultured in S/L exhibit attenuated Mapk signaling, increased  
95 Wnt signaling, and upregulation of transcription factors associated with a naïve-  
96 like state when compared to male ESCs cultured in S/L<sup>9</sup>. Furthermore, female  
97 ESCs cultured in S/L were reported to be hypomethylated at imprinted and non-  
98 imprinted loci<sup>6,10,11</sup>, although the extent of hypomethylation appears to be  
99 variable<sup>12</sup>. We therefore compared the methylation status of our male ESCs with  
100 three isogenic (129S6 x C57BL6 F1) female ESC lines that were cultured in S/L  
101 for 6 passages. At the time of analysis, our female ESC lines retained both X  
102 chromosomes, were hypomethylated globally and at ICRs, and expressed *Impact*  
103 biallelically (Fig. 1d-f and Extended Data Fig. 1i). Unsupervised clustering based  
104 on global methylation levels revealed that S/L-cultured female ESCs clustered  
105 with ICM cells and 2i/L-cultured male ESCs (Fig. 1e). However, when the same  
106 samples were clustered based on ICR methylation levels, female ESCs clustered  
107 with 2i/L-cultured male ESCs but apart from ICM cells and S/L-cultured male  
108 ESCs (Fig. 1f). Moreover, we noticed a substantial overlap between differentially  
109 methylated regions that distinguish male versus female ESCs grown in S/L, and  
110 those that distinguish male ESCs grown in S/L versus 2i/L (Fig. 1g).

111 Concomitant suppression of Mapk signaling and activation of Wnt  
112 signaling may drive additional epigenetic aberrations such as aberrant histone  
113 deposition. Accumulation or loss of the histone variant H2A.X has been shown to  
114 impact the developmental potential of pluripotent stem cells<sup>13</sup>. To examine  
115 whether S/L-cultured female ESCs or 2i/L-cultured male ESCs accumulate  
116 aberrant H2A.X binding patterns, we performed ChIP-Seq for H2A.X. Relative to  
117 S/L-cultured male ESCs, we found that female ESCs and 2i/L-cultured male  
118 ESCs lack H2A.X binding at 38,925 and 51,442 regions, respectively (Extended  
119 Data Fig. 2a-d). Of regions where H2A.X was lost in both male 2i/L-cultured  
120 ESCs and female ESCs (12,179 regions), a significant number of genes  
121 associated with gastrulation, organ development and germ layer formation were  
122 found (Extended Data Fig. 2c-e). Additionally, switching 2i/L-cultured male ESCs  
123 to S/L did not restore the majority of H2A.X binding, suggesting that H2A.X  
124 depletion is irreversible at these sites, similar to ICR methylation (Extended Data  
125 Fig. 2a,b).

126 To determine whether the developmental potential of ESCs is impacted by  
127 the erosion of ICR methylation and/or aberrant H2A.X deposition, we injected the  
128 different ESC lines into 2n or 4n host blastocysts (Fig. 2a and Supplementary  
129 Table 1,2). We found that 2i/L-cultured male ESCs and S/L-cultured female  
130 ESCs gave rise to fewer pups compared to S/L-cultured male ESCs upon 2n  
131 blastocyst injections (Fig. 2b), and several of the pups we obtained displayed  
132 phenotypes associated with aberrant imprinting<sup>14</sup> (inset of Fig. 2b and Extended  
133 Data Fig. 3a). Moreover, adult chimeras derived from 2i/L-cultured male ESCs or  
134 S/L-cultured female ESCs had significantly less agouti coat color, implying a poor  
135 contribution to adult tissues (Fig. 2c). Nevertheless, some low-grade chimeras  
136 produced germline offspring, demonstrating their ability to produce functional  
137 germ cells (Extended Data Fig. 3b). Similarly, both 2i/L-cultured male ESCs and

138 S/L-cultured female ESCs were 5-6 times less efficient at producing entirely  
139 ESC-derived (all-ESC) pups compared to S/L-cultured male ESCs when 4n  
140 blastocyst injections were performed (Fig. 2d and Extended Data Fig. 3c-e).  
141 These results are consistent with a previous report, which showed that early-  
142 passage female ESCs are slightly less effective at producing all-ESC pups  
143 relative to male ESCs<sup>15</sup>. Strikingly however, none of the all-ESC pups generated  
144 from 2i/L-cultured male or S/L-cultured female ESCs survived beyond birth (Fig.  
145 2d and Extended Data Fig. 3d), and our p20 J37 2i/L-cultured ESC line even  
146 failed to generate full term all-ESC pups. J37 ESCs cultured in 2i/L for 16  
147 passages also failed to produce well-differentiated teratomas, suggesting that  
148 mutations acquired in this line compromised their differentiation potential  
149 (Extended Data Fig. 4a,b).

150 Modulation of Wnt/Mapk signaling<sup>2,3</sup>, DNA hypomethylation<sup>4,5</sup>, and H2A.X  
151 loss<sup>16</sup> have been shown to impact genomic stability. We therefore performed  
152 karyotype analysis (Supplementary Table 3) and array Comparative Genomic  
153 Hybridization (aCGH) on our ESC lines cultured in 2i/L. ESCs propagated in 2i/L  
154 for 10 passages had mostly diploid chromosome counts (40,XY) (Fig. 3a, top  
155 row). However, 2i/L-cultured ESC lines at p20 exhibited recurrent chromosomal  
156 aberrations including trisomy 6, 8, 19, and loss of the Y chromosome in many, if  
157 not all cells analyzed, while S/L-cultured ESCs at p20 remained euploid (Fig. 3a-  
158 c and Extended data Fig. 5a). To exclude the possibility that these abnormalities  
159 are specific to our cell lines or culturing techniques, we analyzed a 129/Ola ESC  
160 line that had been independently maintained in 2i/L conditions<sup>17</sup> and found  
161 several chromosomal aberrations including trisomy 6 and 8 (Extended Data Fig.  
162 5b). Additionally, despite previous reports demonstrating that irradiated MEFs do  
163 not affect ESCs in a co-culture system<sup>18</sup>, we passaged one of our ESC lines in  
164 2i/L for 16 passages without feeders. As expected, every cell karyotyped  
165 acquired trisomy 6 and 8, confirming that the 2i/L-derived chromosomal  
166 aberrations are not due to co-culture with MEFs (Extended data Fig. 5c).  
167 Considering these unexpected chromosomal abnormalities, we performed aCGH  
168 on DNA isolated from a rare full term all-ESC pup that was generated using p20  
169 2i/L-cultured ESCs. We did not find evidence for gross copy number  
170 abnormalities in this pup (Extended Data Fig. 5d), even though the parental bulk  
171 cultures had chromosomal aberrations in every cell counted (Fig. 3a middle row,  
172 3b). We surmise that rare euploid ESCs present in the culture experienced a  
173 strong positive selection during development, yet succumbed postnatally due to  
174 the epigenetic aberrations present. To confirm this, we performed RRBS on  
175 cultured explanted keratinocytes derived from chimeric mice produced with 2i/L-  
176 cultured ESCs and found they were hypomethylated at several imprinted loci  
177 (Extended data Fig. 5e).

178 Female ESCs tend to lose one of their two X chromosomes with culture,  
179 thus becoming XO<sup>10</sup>. The loss of an X chromosome in XX ESCs has been  
180 associated with downregulation of naïve-like genes and elevated DNA  
181 methylation, similar to male ESCs cultured in S/L<sup>9,11</sup>. We hypothesized that the  
182 naïve-like state of XX female ESCs—particularly as it relates to decreased Mapk  
183 signaling and increased Wnt signaling—is responsible for the selective pressure

184 to lose an X chromosome. Thus, if the chemical inhibition of Mek1/2 and Gsk3 $\alpha$ / $\beta$   
185 via 2i/L culture attenuates X chromosome loss in female ESCs, we would  
186 conclude that suppressed Mapk signaling and/or elevated Wnt signaling in XX  
187 ESCs drives female ESCs to become XO. To test this hypothesis, we developed  
188 a dual reporter female ESC line (X<sup>G</sup>X<sup>T</sup>) and measured X chromosome loss during  
189 S/L and 2i/L culture (Fig. 3d and Extended data 6a-c). Indeed, when we exposed  
190 X<sup>G</sup>X<sup>T</sup> ESCs to 2i/L, a substantial fraction of GFP/Tomato double-positive cells  
191 persisted relative to X<sup>G</sup>X<sup>T</sup> ESCs cultured in S/L (Fig. 3e).

192 It remains unclear whether Mapk suppression, Wnt activation, or a  
193 combination of these activities is responsible for the epigenetic abnormalities we  
194 observed. Therefore, we performed RRBS on male ESCs cultured in S/L with  
195 one of the two inhibitors used in 2i/L culture: the Mek1/2 inhibitor (S/L+PD) or  
196 Gsk3 $\alpha$ / $\beta$  inhibitor (S/L+CHIR). We found that only ESCs exposed to S/L+PD  
197 acquired methylation levels similar to ESCs cultured in 2i/L (Fig. 4a and  
198 Extended Data Fig. 7a). To confirm these results, we analyzed DNA methylation  
199 levels in male pluripotent stem cells deficient for *Mek1* and *Mek2* (*Mek* DKO) or  
200 *Gsk3 $\alpha$*  and *Gsk3 $\beta$*  (*Gsk3* DKO). We found that *Mek* DKO stem cells are  
201 hypomethylated globally and at ICRs while *Gsk3* DKO stem cells remain largely  
202 unchanged (Fig. 4b,c and Extended Data Fig. 7b). Notably, global methylation,  
203 including at ICR loci, was further reduced in female ESCs cultured in S/L+PD  
204 when compared to female ESCs cultured in S/L (Extended Data Fig. 7c,d).

205 In order to understand how Mek1/2 inhibition induces global  
206 hypomethylation, we performed RNA-sequencing and quantitative large-scale  
207 proteomics of male ESCs cultured in either S/L or S/L+PD for 3 passages (Fig.  
208 4d). PD treatment led to the upregulation of transcription factors that have been  
209 associated with naïve pluripotency (Extended Data Fig. 8a). Additionally, all  
210 major DNA methyltransferases (*Dnmt1*, *Dnmt3a*, *Dnmt3b*) and associated  
211 cofactors (*Dnmt3l*, *Uhrf1*) were downregulated at the RNA and protein level in  
212 PD-treated ESCs (Fig. 4e and Extended Data Fig. 8b). These observations are  
213 consistent with the previous notion that reduced levels of Uhrf1<sup>19</sup> and  
214 Dnmt3a/Dnmt3b<sup>7</sup> underlie 2i/L-induced hypomethylation.

215 We next tested whether Mek1/2 suppression is sufficient to drive the  
216 chromosomal abnormalities we observed in male ESCs cultured in 2i/L.  
217 Karyotypes of our male ESCs cultured in S/L+PD for 16 passages revealed that  
218 every counted cell had some karyotypic abnormality, contrary to ESCs exposed  
219 to S/L+CHIR (Extended Data Fig. 8c,d). To determine whether the genomic  
220 hypomethylation driven by Mek1/2 inhibition in ESCs is sufficient to select for the  
221 recurring karyotypic aberrations, we derived ESCs harboring conditional alleles  
222 for *Dnmt1*, *Dnmt3a* and *Dnmt3b* (*Dnmt* cTKO). When we deleted the Dnmts and  
223 cultured the ESCs in serum for 15 passages, we found that they remained  
224 euploid, suggesting that Mek1/2 suppression drives the selection for certain  
225 chromosomal abnormalities independently of DNA methylation. (Extended Data  
226 Fig. 8e,f).

227 Considering the impact of continual Mek1/2 inhibition on ESCs, we  
228 determined whether previously reported alternative culture conditions lacking  
229 Mek1/2 inhibition<sup>20,21</sup> resemble naïve ESCs while maintaining their

230 developmental potential. We tested two defined media conditions using our  
231 ESCs supplemented with the PKC inhibitor Gö6976 (PKCi/L), or with the Src  
232 inhibitor CGP77675 in combination with CHIR (a2i/L) (Extended data Fig. 9a).  
233 While both PKCi/L and a2i/L conditions were transcriptionally more similar to S/L  
234 than 2i/L, a2i/L-cultured ESCs clustered with 2i/L-cultured ESCs when the ESCs  
235 were grouped using a previously published set of pluripotency and differentiation  
236 genes<sup>22</sup> (Extended Data Fig. 9b-e). RRBS analysis revealed that ESCs cultured  
237 in PKCi/L and a2i/L were globally hypermethylated and retained proper  
238 methylation of ICRs, thus preserving monoallelic expression of *Impact* (Fig. 4f-h  
239 and Extended data Fig. 9f,g). The hypermethylation of a2i/L- and PKCi/L-cultured  
240 ESCs coincided with increased Dnmt3b and Uhrf1 protein levels relative to 2i/L-  
241 cultured ESCs (Fig. 4i). Additionally, when we cultured our female X<sup>G</sup>X<sup>T</sup> ESC line  
242 in a2i/L, we observed an intermediate level of X chromosome loss when  
243 compared to S/L+PD and S/L (Extended data Fig. 9h).

244 We next assessed the developmental potential of PKCi/L- and a2i/L-  
245 cultured ESCs by 4n blastocyst injections. Consistent with the preservation of  
246 monoallelic ICR methylation and euploid karyotype under these conditions, we  
247 were able to generate several germline-competent, adult all-ESC mice using  
248 ESCs cultured in a2i/L for 6 or 16 passages (Fig. 4j,k and Extended data Fig.  
249 9i,j). Unexpectedly, we were able to generate only one adult all-ESC mouse  
250 using ESCs cultured in PKCi/L for 6 passages (Fig. 4j,k), even though these  
251 ESCs maintained monoallelic ICR methylation and remained euploid (Extended  
252 data Fig 9k). It is unclear as to why these PKCi/L generated so few all-ESC mice,  
253 however by p20 in PKCi/L, these ESCs did select for a large duplication on  
254 chromosome 1 (Fig 9i and Extended data Fig 9k).

255 Different conditions have recently been discovered that allow for the  
256 propagation of naïve human ESCs<sup>23,24</sup>. Similar to 2i/L-cultured mouse ESCs,  
257 naïve human ESCs are globally hypomethylated, lose ICR methylation, and  
258 acquire karyotypic abnormalities<sup>25</sup>. Since inhibition of MEK1/2 via PD is common  
259 among current naïve human culture conditions, we modified the naïve media  
260 “t2iLGöY”<sup>26</sup> by replacing PD with the Src inhibitor used in a2i/L culture (termed  
261 a2iLGöY). We then monitored the maintenance of the naïve state in human  
262 ESCs carrying a naïve-specific  $\Delta$ PE-OCT4-EGFP reporter<sup>23</sup> upon exposure to  
263 t2iLGöY or a2iLGöY. As expected, t2iLGöY maintained GFP expression in the  
264 majority of  $\Delta$ PE-OCT4-EGFP ESCs. However, exposure of  $\Delta$ PE-OCT4-EGFP  
265 ESCs to a2iLGöY led to a rapid loss OCT4-GFP expression and differentiation,  
266 indicating that SRC inhibition cannot replace MEK1/2 inhibition in this culture  
267 system (Extended Data Fig. 10a,b).

268 Our results demonstrate that attenuation of Mapk signaling via Mek1/2  
269 suppression is sufficient to induce global hypomethylation of DNA in ESCs, thus  
270 recapitulating the naïve epigenetic state within the ICM. Based on our data, we  
271 suggest that the levels of Mapk signaling capture distinct epigenetic states  
272 ranging from the naïve state that resembles the ICM to the primed state that  
273 resembles the post-implantation epiblast. While inhibition of Mek1/2 maintains  
274 ESCs in a naïve epigenetic state, inhibition of Src appears to maintain ESCs in  
275 an epigenetic state that lies in between naïve and primed (Fig 4m). Considering

276 that Mek1/2 inhibition suppresses Mapk signaling to a greater extent than Src  
277 inhibition<sup>21</sup>, our results imply that the degree of Mapk signaling dictates the  
278 epigenetic state and chromosomal stability of ESCs. Comparing targets of  
279 Mek1/2 and Src will be informative to understand how Mapk signaling facilitates  
280 the capture of different epigenetic states as well as drive the selection of  
281 particular chromosomal aberrations in pluripotent stem cells. These comparative  
282 studies should also provide valuable insights into the epigenetic regulation of  
283 early embryonic development and may lead to strategies to generate stable,  
284 human naïve ESCs.

285

## 286 **METHODS**

287

### 288 **Animal care and use**

289 All mice used in the study were housed and bred in Specific Pathogen Free  
290 (SPF) rooms located in the AAALAC-accredited Center for Comparative  
291 Medicine vivarium at Massachusetts General Hospital. All mice were housed in  
292 ventilated cages on a standard 12:12 light cycle. All procedures involving mice  
293 adhered to the guidelines of the approved Massachusetts General Hospital  
294 Institutional Animal Care and Use Committee (IACUC) protocol no.  
295 2006N000104.

296

### 297 **ESC derivation and cell culture**

298 Blastocysts were isolated from the uterine horns of pregnant females at 3.5 dpc  
299 using a dissection microscope. Individual blastocysts were plated onto feeder  
300 cells in 2i/L medium and cultured for 7 days. Emerging ICM outgrowths were  
301 directly picked into S/L medium on feeders to establish stable ESC lines as  
302 previously reported<sup>11</sup>. ESC lines were maintained by dissociating cells with  
303 0.25% trypsin every 4 days and re-plating them onto irradiated MEFs. S/L  
304 medium contains KO DMEM (Invitrogen) supplemented with 15% FBS (Hyclone),  
305 1mM L-glutamine, 100 µM non-essential amino acids (Invitrogen), 1X PenStrep  
306 (Invitrogen), 0.1 mM beta-mercaptoethanol (Invitrogen), and 10<sup>3</sup> IU LIF (in  
307 house). 2i/L medium contains a 1:1 mixture of DMEM/F12 supplemented with N2  
308 (Invitrogen) and Neurobasal media with glutamine (Invitrogen) supplemented  
309 with B27 (Invitrogen), 1X PenStrep (Invitrogen), 10<sup>3</sup> IU LIF (in house), 1 µM  
310 PD0325901 (Tocris) and 3 µM CHIR99021 (Tocris). a2i/L medium contains a 1:1  
311 mixture of DMEM/F12 supplemented with N2 (Invitrogen) and Neurobasal media  
312 with glutamine (Invitrogen) supplemented with B27 (Invitrogen), 1X PenStrep  
313 (Invitrogen), 10<sup>3</sup> IU LIF (in house), 1.5 µM CGP77675 (Tocris) and 3 µM  
314 CHIR99021 (Tocris). PKCi/L medium contains a 1:1 mixture of DMEM/F12  
315 supplemented with N2 (Invitrogen) and Neurobasal media with glutamine  
316 (Invitrogen) supplemented with B27 (Invitrogen), 1X PenStrep (Invitrogen), 10<sup>3</sup> IU  
317 LIF (in house) and 5 µM Gö6976 (Tocris). Irradiated MEFs were used for all  
318 culture media to ensure consistent conditions, unless noted. All lines were  
319 periodically tested for Mycoplasma using the Lonza mycoalert kit and found to be  
320 negative.

321



322 **iPSC generation**  
323 *Mek1<sup>fl/fl</sup>;Mek2<sup>-/-</sup>* or F1 *Mus musculus* x *Mus spretus* MEFs were transduced with  
324 lentiviruses that facilitate the constitutive expression of M2rtTA and inducible  
325 expression of Oct4, Klf4, Sox2 and c-Myc<sup>27</sup>. Infected MEFs were plated onto  
326 irradiated MEF feeders in S/L media supplemented with 2 µg/ml doxycycline until  
327 iPSC colonies emerged. Doxycycline-independent, clonal iPSCs were picked and  
328 expanded. To remove the floxed *Mek1* allele to generate *Mek1/2* DKO iPSCs, we  
329 transiently transfected via electroporation a plasmid driving Cre recombinase and  
330 subcloned. *Mek1/2* double knock-out iPSCs were verified by Western blot and  
331 maintained on irradiated MEF feeders in S/L.

332  
333 **Generation of *Dnmt1/3a/3b* triple knock out (TKO) ESCs.**  
334 *Dnmt* cTKO ESCs were generated as described using blastocysts obtained from  
335 a *Dnmt1<sup>fl/fl4</sup>*, *Dnmt3a<sup>fl/fl28</sup>* and *Dnmt3b<sup>fl/fl29</sup>* intercross. To remove the floxed alleles,  
336 we transiently transfected via electroporation a plasmid driving Cre recombinase  
337 and subcloned. *Dnmt* TKO ESCs were verified by Western blot and maintained  
338 on irradiated MEF feeders in S/L.

339  
340  
341 **Reduced representation bisulfite sequencing (RRBS)**  
342 Genome-wide basepair-level methylation was assayed using Reduced  
343 Representation Bisulfite Sequencing (RRBS)<sup>30</sup>. Briefly, genomic DNA was  
344 digested using the *MspI* restriction enzyme and subjected to bisulfite treatment,  
345 which converts unmethylated cytosine residues to uracil. Genomic fragments  
346 were sequenced using next-generation sequencing, and aligned to the mm9  
347 reference genome. Methylation levels of individual CpGs were measured by  
348 observing bisulfite conversion in the aligned read as compared to the reference  
349 genome. On average, 1.596M CpGs were covered per sample, at a mean depth  
350 of 14.31 reads/CpG.

351 Region-level methylation values were computed by pooling coverage-  
352 weighted methylation levels in CpGs that were measured by at least 3 reads in  
353 80% of samples. A consensus set of regions was defined using regions that had  
354 at least 5 reads in every sample. Genomic methylation plots used methylation  
355 levels of 127,671 non-overlapping 1kb tiles. Heatmaps show methylation levels  
356 of 1kb tiles clustered using k-means clustering (k=5), and samples clustered by  
357 hierarchical clustering. Promoters were defined as 1kb up- and downstream from  
358 RefSeq transcription start sites. LINEs, SINEs, LTRs and IAPs were defined  
359 using RepBase. ICRs were defined as a set of 17 canonical ICRs covered by  
360 RRBS as used in<sup>31</sup>.

361 Violin plots were created using the 'vioplot' R package. The white dot  
362 represents the median. The box extends from the 25th percentile to the 75th  
363 percentile of the data (the interquartile range). Whiskers extend from the box to  
364 the most extreme data point, which is no more than 1.5 times the interquartile  
365 range. Heatmaps were created using the 'pheatmap' R package and clustering  
366 was performed using euclidean distance and complete linkage.

367

368 **RNA-sequencing and analysis**

369 RNA-Seq libraries were constructed from RiboZero-selected RNA using  
370 NEBNext Ultra Directional RNA Library Prep Kit for Illumina (New England  
371 Biolabs) and sequenced on an Illumina HiSeq2500 instrument. Transcriptome  
372 mapping was performed with STAR version 2.3.0<sup>32</sup> using the Ensembl 67 release  
373 exon/splice-junction annotations. Approximately 55-90% of reads mapped  
374 uniquely. Read counts for individual genes were produced using the unstranded  
375 count feature in HTSeq v.0.6.0<sup>33</sup>. Differential expression analysis was performed  
376 using the exactTest routine of the edgeR package<sup>34</sup> after normalizing read counts  
377 and including only those genes with cpm > 1 for one or more samples<sup>35</sup>.  
378 Differentially expressed genes were defined based on the criteria of >2-fold  
379 change in expression value and false discovery rate (FDR) < 0.05.  
380 Allelic expression asymmetry was quantified via samtools mpileup at exonic SNP  
381 sites that differentiated C57B6 from 129S6 reference genomes (indels  
382 excluded)<sup>36</sup>. To measure allelic asymmetry in expression, we used the  
383 asymmetry metric calculated as the ratio  $(129S6 - C57B6)/(129S6 + C57B6)$ ,  
384 where 129S6 and C57B6 are the numbers of reads assigned at a given SNP to  
385 129S6 and C57B6 allele, respectively. This measure of allelic asymmetry ranges  
386 from -1 (C57B6 only) to 1 (129S6 only), with 0 corresponding to fully balanced  
387 biallelic expression.

388

389 **RNA-seq and analysis of Interspecific iPSCs.**

390 Total RNA specimens were isolated from the interspecific iPSCs using (please  
391 specify kits or methods), and their integrity [RNA Integrity Numbers (RIN)  $\geq 9.4$ ]  
392 was confirmed using Agilent TapeStation with RNA High Sensitivity tapes.  
393 Illumina sequencing libraries with 6-bp single index were constructed from 1 ug  
394 total RNA using the TruSeq Standard Total RNA LT kit with the Ribo-Zero Gold  
395 ribosomal RNA depletion module (Illumina). Libraries were subjected to size  
396 distribution analysis (200 – 500 bp, peaking at 280-290 bp) using TapeStation  
397 with the High Sensitivity D1000 tapes and quantified using the Illumina library  
398 qPCR quantification kit (KAPA Biosystems). Equal concentrations (4 nM) of  
399 libraries were pooled and subjected to Illumina NextSeq deep sequencing using  
400 High Output Sequencing Kit version 2 (paired-end, 75 nt + 75 nt). The fastq  
401 format raw reads data files were generated by the Illumina BaseSpace  
402 Sequencing Hub and subjected to pre-alignment quality control using the fastQC  
403 software (Babraham Institute). The fastq reads were aligned to the  
404 GRCm38/mm10 *Mus musculus musculus* (C57BL/6) reference genome  
405 sequence using the STAR aligner (version 2.4.2.a) with the UCSC annotation  
406 GTF file and the sjdbOverhang parameter 74 for genome indexing and  
407 alignment. The aligned reads were sorted and subjected to duplicates removal  
408 using the sambamba<sup>37</sup> implementation of SAMtools<sup>38</sup>, resulting in 82-95  
409 uniquely-mapped reads per RNA specimen. These reads were assigned to  
410 mm10-annotated genes and counted using the Bioconductor package  
411 Rsubread<sup>33</sup> (69.1-71.2% successfully assigned reads), and the gene counts were  
412 normalized to generate the cpm (counts per million reads) values using the  
413 negative binomial distribution model implemented by edgeR<sup>35</sup>. Tracks of the

414 uniquely mapped reads were directly inspected using the Integrative Genomics  
415 Viewer<sup>39</sup>, which reports paternal (*M. spretus*) and maternal (*mm10* – *Mus*  
416 *musculus musculus*) allelic counts for each SNP. Statistical significance of Allelic  
417 counts at multiple SNPs in each gene were examined by *t*-test (unpaired, two-  
418 tail, homoscedastic assumption).

419

### 420 **Whole-genome sequencing**

421 Genomic DNA (1 ug) was sonicated using a Covaris S2 sonicator (Covaris) to  
422 ~350 bp peak fragments. To avoid PCR-derived bias of read counts, gDNA  
423 fragments were subjected to PCR-free synthesis of Illumina NextSeq deep  
424 sequencing libraries with the i7 index using the TruSeq DNA PCR-free LT  
425 Sample Preparation Kit - Set A (Illumina). Libraries were quantified using KAPA  
426 Illumina library quantification qPCR kit (KAPA Biosystems), and equal  
427 concentrations (4 nM) of libraries were pooled. Size distributions of gDNA  
428 fragments and deep sequencing libraries were examined using Agilent  
429 TapeStation with Genomic DNA screening tapes (Agilent Technologies). Single-  
430 read deep sequencing (76 nt) was performed using Illumina NextSeq 500  
431 sequencer with the high output v2 kit. Fastq files were subjected to a quality  
432 control process using Trim Galore! and fastQC (Babraham Institute), which  
433 excluded raw quality reads (Phred score < 20) and deleted the Illumina adaptor  
434 sequences and the last one nucleotide at the 3' end to avoid nucleotide base  
435 biases. The trimmed/QCed fastq reads were aligned to the mouse  
436 GRCm38/mm10 reference genome sequence using the STAR aligner (ver.  
437 2.4.2.a) with the genomic DNA alignment configuration, generating the bam  
438 format aligned reads files. The reads were extracted using the sambamba  
439 toolkit<sup>37</sup>. Numbers of the uniquely mapped reads were 46.2 – 59.6 million per  
440 sample, which corresponded to about 1.2X ~ 1.6X average depth of genome  
441 coverage. Reads assigned to each chromosome are counted to generate cnt  
442 files. The chromosome count data were subjected to ploidy analysis, as  
443 previously described<sup>40</sup>.

444

### 445 **Native Chromatin immunoprecipitation (N-ChIP)**

446 N-ChIP assay was performed as previously described<sup>41</sup>. Briefly, approximately  
447 10 million ESCs were used for each ChIP and massive parallel sequencing  
448 (ChIP-Seq) experiment. Chromatin pellets were briefly digested with MNase  
449 (New England BioLabs) and the mononucleosomes were monitored by  
450 electrophoresis 0.5ug anti-H2A.X antibody (active motif 39689) was used per  
451 ChIP experiment. Co-purified DNA and whole cell extraction (WCE) input  
452 genomic DNA were subject to library construction, cluster generation and next-  
453 generation sequencing (Illumina Genome Analyzer II and HiSeq 2000). The  
454 output sequencing reads were filtered and pre-analyzed with Illumina standard  
455 workflow. After filtration, the qualified tags (in fastq format) were aligned to the  
456 mouse genome (mm9) with bowtie2 (2.0.6)<sup>42</sup>. Reads mapped to sex  
457 chromosomes were discarded. Aligned reads were used for peak calling using  
458 the RSEG algorithm (0.4.8) in mode 3 to identify differential binding regions  
459 relative to J34 S/L samples<sup>43</sup>. For cells cultured in 2i/L and then switched back to

460 serum, the combination of all male S/L samples were used as control to reach a  
461 comparable throughput. The relative decreased regions were assigned to whole  
462 genome-wide 20kb windows to calculate a weighted average score and used for  
463 enumerating overlapping regions. Heatmap and unsupervised hierarchical  
464 clustering analysis were drawn in 500kb domains. GREAT was used to predict  
465 the putative target genes statistical relevance of associations between genomic  
466 regions and annotations<sup>44</sup>.

467

### 468 **Blastocyst injections**

469 Blastocyst (2n and 4n) injections were performed as previously described<sup>45</sup>.  
470 Briefly, female BDF1 mice were superovulated by intraperitoneal injection with  
471 PMS and hCG and mated to BDF1 stud males. Zygotes were isolated from  
472 females with a vaginal plug 24 h after hCG injection. For 2n injections, zygotes  
473 were cultured *in vitro* for 3 d in KSOM medium, and resultant blastocysts were  
474 injected with 10-15 ESCs before transfer into pseudopregnant recipient females.  
475 When newborn pups were not delivered until day 18 after the transfer, resorbed  
476 embryos were counted from the uteri of the recipient females and counted as  
477 “Resorption”. Surviving neonates with regular breathing was termed “Breathing”  
478 and two weeks later their chimerism was assessed based on their agouti coat  
479 color contributions.

480 For 4n injections, zygotes were cultured overnight until they reached the  
481 2-cell stage, at which point they were electrofused. After 1 h, fused 1-cell  
482 embryos were carefully identified and separated from embryos that had failed to  
483 fuse, cultured in KSOM for another 2 d, and then injected with 15-20 ESCs  
484 before embryo transfer. C-section was performed at day 17 after the embryo  
485 transfer and embryos were termed “Full-term”, “Breathing” and “Adult” when they  
486 reached the full-term, established regular breathing after birth and survived past  
487 5 weeks, respectively.

488

### 489 **Teratoma assay**

490 ESCs were grown to confluency in a single well of a confluent six well plate. Cells  
491 were then trypsinized and counted.  $2 \times 10^6$  ESCs were resuspended in 300  $\mu$ L of  
492 ESC media and injected subcutaneously into the flanks of a nu/nu  
493 immunocompromised mouse. Teratomas were monitored and removed once  
494 tumor size reached 1 cm or tumors became ulcerated. Tumors were then  
495 weighed and processed for hematoxylin and eosin staining. Analysis of the  
496 tumor sections were blindly scored for the presence of each germ layer.

497

### 498 **Array Comparative genomic hybridization (aCGH)**

499 Genomic DNA was isolated from frozen cell pellets using DNeasy tissue kit  
500 (Qiagen) following the manufacturer’s protocol. Concentration and quality of  
501 isolated genomic DNA was assessed using a spectrophotometer (NanoDrop  
502 Technologies, Wilmington, DE) to assure absence of contaminating protein  
503 (260/A280 ratio is greater than or equal to 1.8) and absence of carbohydrate,  
504 lipid and residual phenol (260/A230 ratio greater than or equal to 2.0). Integrity of  
505 genomic DNA was confirmed by low voltage 0.6% agarose gel electrophoresis

506 with mean band size of about 50Kb. Sample labeling was performed following  
507 Agilent's recommendation for array CGH. Briefly, 1.5 µg of genomic DNA was  
508 digested with 5 units of Alu I and Rsa I (Promega) for 2 hours at 37°C. Labeling  
509 reactions were carried out with total amount of fragmented DNA for 3 hours at  
510 37C using a BioPrime Array CGH Genomic Labeling Module (Invitrogen) with 3  
511 umol Cy5-dUTP or Cy3-dUTP (Perkin Elmer). Labeled samples were purified,  
512 concentrated on a Centricon YM-30 column (Millipore), and then mixed with 10x  
513 blocking agent and 2x hybridization buffer (Agilent Technologies). Samples were  
514 then hybridized on a SurePrint G3 Mouse 4x 180K CGH Microarray chip that  
515 contains 170,305 distinct biological probes taken from the mouse genome.  
516 Hybridized arrays were imaged with Agilent G2565BA microarray scanner using  
517 default settings. Data were extracted and analyzed using Agilent's Genome  
518 Workbench software. Aberrant regions (gains or losses) were identified using a  
519 build-in ADM-2 algorithm with aberration filter setting as minimum number of  
520 probes for gains or losses  $\geq 20$  and absolute log<sub>2</sub> ratio for gains or losses  $\geq$   
521 0.35.

522

### 523 **Karyotyping**

524 Mouse ESC lines were prepared for cytogenetic analysis by treatment with  
525 colcemid (Irvine Scientific, Santa Ana, CA) at a final concentration of 0.1 µg/ml  
526 for 3 hours to accumulate cells in metaphase. Cells were then exposed to 0.075  
527 M KCl for 25 minutes at 37°C and fixed with 3:1 methanol:acetic acid. Air-dried  
528 slides were generated and G-banded following standard GTG banding protocols.  
529 Two levels of analysis were pursued: for all lines, a minimum of 10 metaphase  
530 cells were counted, and 2-4 karyotypes prepared. For lines with a normal or  
531 consistent straightforward result, no further analysis was done. For lines with a  
532 complex karyotype, additional metaphases were counted (total 20), and 10  
533 karyotypes prepared to better characterize the variability.

534

### 535 **Generation of X<sup>G</sup>X<sup>T</sup> ESC line**

536 X<sup>G</sup>X<sup>T</sup> lines were generated by CRISPR/Cas mediated gene targeting in a newly  
537 derived 129SvJ x C57B6 F1 ESC line. Two homology constructs were designed  
538 to integrate either E2A-GFP-T2A-Neo<sup>R</sup>-STOP or E2A-Tomato-T2A-Puro<sup>R</sup>-STOP  
539 in frame with the last exon of *Hprt*. The constructs were generated via PCR  
540 amplification and Gibson assembly (New England Biolabs) of the respective  
541 fluorescent protein and resistance marker flanked on either end by 500bp of  
542 homology to the *Hprt* locus. An sgRNA was designed targeting the last exon of  
543 *Hprt*. Both homology constructs, the sgRNA and a construct containing Cas9  
544 were cotransfected into early passage female ESCs with Lipofectamine 2000  
545 (Thermo Fisher). Following transfection, dual selection with G418 and puromycin  
546 was applied for 10-14 days. Resistant clones were picked and targeting was  
547 confirmed by Southern blot.

548

### 549 **Dot blot analysis for 5mC**

550 Genomic DNA samples were prepared with 2-fold serial dilutions in TE buffer and  
551 then denatured in 0.4 M NaOH/10 mM EDTA at 95°C for 10 min and followed by

552 adding an equal volume of cold 2 M ammonium acetate (pH 7.0). Denatured  
553 DNA samples were spotted on a nitrocellulose membrane in an assembled Bio-  
554 Dot apparatus (Bio-Rad) according to the manufacturer's protocol. The  
555 membrane was washed with 2X SSC buffer and UV-crosslinked for 10 min. The  
556 membrane was then blocked with 5% non-fat milk for 1 hr and incubated with an  
557 anti-5mC antibody (Active Motif; 39649), washed, and then incubated with an  
558 HRP-conjugated secondary antibody. Chemiluminescence was measured, and  
559 subsequently stained with methylene blue to detect the quantity of DNA loaded.  
560 Quantification was performed by image-J software analysis.

561

### 562 **Mass spectrometry analysis**

563 Mass spectrometry analyses were performed on an Orbitrap Fusion Lumos mass  
564 spectrometer (ThermoFisher Scientific) coupled to an Easy-nLC 1200 ultra-high  
565 pressure liquid chromatography (LC) pump (ThermoFisher Scientific). Peptides  
566 were separated at 300 nL/min using a self-packed analytical column (75  $\mu$ m inner  
567 diameter) that was packed with 0.5 cm of Magic C18 resin (5  $\mu$ m, 100  $\text{\AA}$ ,  
568 Michrom Bioresources) followed by 35 cm of Sepax Technologies GP-C18 resin  
569 (1.8  $\mu$ m, 120  $\text{\AA}$ ). LC buffers consisted of 0.1% formic acid (buffer A) and 80%  
570 ACN with 0.1% formic acid and LC gradients were optimized to ensure equal  
571 elution of peptides throughout the analysis. Intact mass analysis of peptides  
572 (MS1) was performed in the Orbitrap (AGC target 1e6, 120,000 resolution, 100  
573 ms maximum injection time) and used to select the 10 most abundant features  
574 for MS/MS (MS2) analysis. Candidate peaks were filtered based on charge state  
575  $\geq 2$  and monoisotopic peak assignment, and dynamic exclusion (60 second  $\pm$  7.5  
576 ppm) was enabled. Additionally, only one charge state was selected for each  
577 precursor for analysis of non-phosphorylated peptides. Each precursor was  
578 isolated with using a quadrupole mass filter (0.5 Th width) and then fragmented  
579 with collision-induced dissociation (CID, 35 NCE) ion the ion trap with distinct  
580 settings for non-phosphorylated (AGC target =  $2.5 \times 10^4$ , maximum injection time  
581 = 200 ms) peptides. To alleviate the effects of precursor ion interference multiple  
582 fragment ions were isolated using synchronous precursor selection (SPS) prior to  
583 HCD (55 NCE, SPS notches = 8, AGC target =  $2.2 \times 10^5$ , maximum injection time  
584 of 150 ms for non-phosphorylated peptides) MS3 fragmentation and Orbitrap  
585 analysis (50,000 resolution).

586

### 587 **Mass spectrometry data analysis**

588 A compilation of in-house software was used to convert mass spectrometric data  
589 (Thermo ".raw" files) to mzXML format, as well as to correct monoisotopic m/z  
590 measurements and erroneous peptide charge state assignments<sup>46</sup>. Assignment  
591 of MS/MS spectra was performed using the SEQUEST algorithm<sup>47</sup>. Static  
592 modifications included TMT (229.16293 Da) on both the n-terminus of peptides  
593 and lysine residues and carbamidomethylation of cysteine residues (57.02146  
594 Da). Peptide spectral matches were filtered to 1% false discovery rate (FDR)  
595 using the target-decoy strategy<sup>48</sup>, before being grouped into proteins which were  
596 then filtered to 1% FDR at the protein level as previously described<sup>46</sup>. All data  
597 analysis was performed using R.

598

599 **Western blot analysis**

600 Cells were lysed in modified RIPA buffer [50 mM Tris·HCl, pH 8, 150 mM NaCl,  
601 0.1% SDS, 0.5% sodium deoxycholate, 1% Triton X-100, 1 mM EDTA, 1×  
602 protease inhibitor mixture (Roche Diagnostics), 1× PhosSTOP phosphatase  
603 inhibitors (Roche Diagnostics), 0.01 U/μL benzonase (Novagen)]. Cell lysate was  
604 then sonicated for five 30-second pulses (with 30 second pauses) in a bath  
605 sonicator at 4°C (Diagenode). Lysates were cleared of cell debris by  
606 centrifugation at 20,000 × g for 5 minutes. Westerns were performed with anti-  
607 Dnmt1 (1:500 dilution; Cell Signaling, 5119S), anti-Uhrf1 (1:200 dilution; Santa  
608 Cruz, sc-98817), anti-Dnmt3a (1:500 dilution; Santa Cruz Biotechnology, 20703),  
609 anti-Dnmt3b (1:1000 dilution; Abcam, 13604), or anti-β-Actin (1:10,000 dilution;  
610 Cell Signaling Technology, 5125S).

611

612 **Data Availability Statement**

613 The accession number for the raw data files for the RRBS analysis reported in  
614 this paper is NCBI GEO: GSE97995

615

616 The accession number for the raw data files for the RRBS analysis on female  
617 ESC lines is NCBI GEO: GSM1679872, GSM1679873, GSM1679874

618

619 The accession number for the raw data files for the RNA-seq analysis reported in  
620 this paper is NCBI GEO: GSE97954, GSE93103

621

622 The accession number for the raw data files for the Genome-sequencing analysis  
623 reported in this paper is NCBI SRA: SRP102419

624

625 The accession number for the raw data files for the ChIP-seq analysis reported in  
626 this paper is NCBI GEO: GSE98771

627

628

629 **REFERENCES**

630

- 631 1. Ying, Q.-L. *et al.* The ground state of embryonic stem cell self-renewal.  
632 *Nature* **453**, 519–523 (2008).
- 633 2. Raggioli, A., Junghans, D., Rudloff, S. & Kemler, R. Beta-catenin is vital for  
634 the integrity of mouse embryonic stem cells. *PLoS ONE* **9**, e86691 (2014).
- 635 3. Chen, H. *et al.* Erk signaling is indispensable for genomic stability and self-  
636 renewal of mouse embryonic stem cells. *Proc. Natl. Acad. Sci. U.S.A.* **112**,  
637 E5936–43 (2015).
- 638 4. Chen, R. Z., Pettersson, U., Beard, C., Jackson-Grusby, L. & Jaenisch, R.  
639 DNA hypomethylation leads to elevated mutation rates. *Nature* **395**, 89–93  
640 (1998).
- 641 5. Gaudet, F. *et al.* Induction of tumors in mice by genomic hypomethylation.  
642 *Science* **300**, 489–492 (2003).
- 643 6. Habibi, E. *et al.* Whole-genome bisulfite sequencing of two distinct

- 644 interconvertible DNA methylomes of mouse embryonic stem cells. *Cell*  
645 *Stem Cell* **13**, 360–369 (2013).
- 646 7. Ficzb, G. *et al.* FGF signaling inhibition in ESCs drives rapid genome-wide  
647 demethylation to the epigenetic ground state of pluripotency. *Cell Stem*  
648 *Cell* **13**, 351–359 (2013).
- 649 8. Leitch, H. G. *et al.* Naive pluripotency is associated with global DNA  
650 hypomethylation. *Nat. Struct. Mol. Biol.* **20**, 311–316 (2013).
- 651 9. Schulz, E. G. *et al.* The two active X chromosomes in female ESCs block  
652 exit from the pluripotent state by modulating the ESC signaling network.  
653 *Cell Stem Cell* **14**, 203–216 (2014).
- 654 10. Zvetkova, I. *et al.* Global hypomethylation of the genome in XX embryonic  
655 stem cells. *Nat. Genet.* **37**, 1274–1279 (2005).
- 656 11. Choi, J. *et al.* DUSP9 Modulates DNA Hypomethylation in Female Mouse  
657 Pluripotent Stem Cells. *Cell Stem Cell* **20**, 706–719.e7 (2017).
- 658 12. Hackett, J. A. *et al.* Synergistic mechanisms of DNA demethylation during  
659 transition to ground-state pluripotency. *Stem Cell Reports* **1**, 518–531  
660 (2013).
- 661 13. Wu, T. *et al.* Histone variant H2A.X deposition pattern serves as a  
662 functional epigenetic mark for distinguishing the developmental potentials  
663 of iPSCs. *Cell Stem Cell* **15**, 281–294 (2014).
- 664 14. Plasschaert, R. N. & Bartolomei, M. S. Genomic imprinting in development,  
665 growth, behavior and stem cells. *Development* **141**, 1805–1813 (2014).
- 666 15. Nagy, A., Rossant, J., Nagy, R., Abramow-Newerly, W. & Roder, J. C.  
667 Derivation of completely cell culture-derived mice from early-passage  
668 embryonic stem cells. *Proc. Natl. Acad. Sci. U.S.A.* **90**, 8424–8428 (1993).
- 669 16. Celeste, A. *et al.* H2AX haploinsufficiency modifies genomic stability and  
670 tumor susceptibility. *Cell* **114**, 371–383 (2003).
- 671 17. Wray, J. *et al.* Inhibition of glycogen synthase kinase-3 alleviates Tcf3  
672 repression of the pluripotency network and increases embryonic stem cell  
673 resistance to differentiation. *Nat. Cell Biol.* **13**, 838–845 (2011).
- 674 18. Tamm, C., Pijuan Galitó, S. & Annerén, C. A comparative study of  
675 protocols for mouse embryonic stem cell culturing. *PLoS ONE* **8**, e81156  
676 (2013).
- 677 19. Meyenn, von, F. *et al.* Impairment of DNA Methylation Maintenance Is the  
678 Main Cause of Global Demethylation in Naive Embryonic Stem Cells. *Mol.*  
679 *Cell* **62**, 983 (2016).
- 680 20. Dutta, D. *et al.* Self-renewal versus lineage commitment of embryonic stem  
681 cells: protein kinase C signaling shifts the balance. *Stem Cells* **29**, 618–628  
682 (2011).
- 683 21. Shimizu, T. *et al.* Dual inhibition of Src and GSK3 maintains mouse  
684 embryonic stem cells, whose differentiation is mechanically regulated by  
685 Src signaling. *Stem Cells* **30**, 1394–1404 (2012).
- 686 22. Kolodziejczyk, A. A. *et al.* Single Cell RNA-Sequencing of Pluripotent  
687 States Unlocks Modular Transcriptional Variation. *Cell Stem Cell* **17**, 471–  
688 485 (2015).
- 689 23. Theunissen, T. W. *et al.* Systematic identification of culture conditions for



- 690 induction and maintenance of naive human pluripotency. *Cell Stem Cell* **15**,  
691 471–487 (2014).
- 692 24. Takashima, Y. *et al.* Resetting transcription factor control circuitry toward  
693 ground-state pluripotency in human. *Cell* **158**, 1254–1269 (2014).
- 694 25. Pastor, W. A. *et al.* Naive Human Pluripotent Cells Feature a Methylation  
695 Landscape Devoid of Blastocyst or Germline Memory. *Cell Stem Cell* **18**,  
696 323–329 (2016).
- 697 26. Takashima, Y. *et al.* Resetting transcription factor control circuitry toward  
698 ground-state pluripotency in human. *Cell* **158**, 1254–1269 (2014).
- 699 27. Stadtfeld, M., Maherali, N., Borkent, M. & Hochedlinger, K. A  
700 reprogrammable mouse strain from gene-targeted embryonic stem cells.  
701 *Nat. Methods* **7**, 53–55 (2010).
- 702 28. Kaneda, M. *et al.* Essential role for de novo DNA methyltransferase  
703 Dnmt3a in paternal and maternal imprinting. *Nature* **429**, 900–903 (2004).
- 704 29. Dodge, J. E. *et al.* Inactivation of Dnmt3b in mouse embryonic fibroblasts  
705 results in DNA hypomethylation, chromosomal instability, and spontaneous  
706 immortalization. *J. Biol. Chem.* **280**, 17986–17991 (2005).
- 707 30. Boyle, P. *et al.* Gel-free multiplexed reduced representation bisulfite  
708 sequencing for large-scale DNA methylation profiling. *Genome Biol.* **13**,  
709 R92 (2012).
- 710 31. Meissner, A. *et al.* Genome-scale DNA methylation maps of pluripotent and  
711 differentiated cells. *Nature* **454**, 766–770 (2008).
- 712 32. Anders, S., Pyl, P. T. & Huber, W. HTSeq—a Python framework to work  
713 with high-throughput sequencing data. *Bioinformatics* **31**, 166–169 (2015).
- 714 33. Anders, S. *et al.* Count-based differential expression analysis of RNA  
715 sequencing data using R and Bioconductor. *Nat Protoc* **8**, 1765–1786  
716 (2013).
- 717 34. Dobin, A. *et al.* STAR: ultrafast universal RNA-seq aligner. *Bioinformatics*  
718 **29**, 15–21 (2013).
- 719 35. Robinson, M. D., McCarthy, D. J. & Smyth, G. K. edgeR: a Bioconductor  
720 package for differential expression analysis of digital gene expression data.  
721 *Bioinformatics* **26**, 139–140 (2010).
- 722 36. Keane, T. M. *et al.* Mouse genomic variation and its effect on phenotypes  
723 and gene regulation. *Nature* **477**, 289–294 (2011).
- 724 37. Tarasov, A., Vilella, A. J., Cuppen, E., Nijman, I. J. & Prins, P. Sambamba:  
725 fast processing of NGS alignment formats. *Bioinformatics* **31**, 2032–2034  
726 (2015).
- 727 38. Li, H. *et al.* The Sequence Alignment/Map format and SAMtools.  
728 *Bioinformatics* **25**, 2078–2079 (2009).
- 729 39. Robinson, J. T. *et al.* Integrative genomics viewer. *Nat. Biotechnol.* **29**, 24–  
730 26 (2011).
- 731 40. Treff, N. R. *et al.* Next Generation Sequencing-Based Comprehensive  
732 Chromosome Screening in Mouse Polar Bodies, Oocytes, and Embryos.  
733 *Biol. Reprod.* **94**, 76 (2016).
- 734 41. Xiao, A. *et al.* WSTF regulates the H2A.X DNA damage response via a  
735 novel tyrosine kinase activity. *Nature* **457**, 57–62 (2009).

- 736 42. Langmead, B., Trapnell, C., Pop, M. & Salzberg, S. L. Ultrafast and  
737 memory-efficient alignment of short DNA sequences to the human  
738 genome. *Genome Biol.* **10**, R25 (2009).
- 739 43. Song, Q. & Smith, A. D. Identifying dispersed epigenomic domains from  
740 ChIP-Seq data. *Bioinformatics* **27**, 870–871 (2011).
- 741 44. McLean, C. Y. *et al.* GREAT improves functional interpretation of cis-  
742 regulatory regions. *Nat. Biotechnol.* **28**, 495–501 (2010).
- 743 45. Eggan, K. *et al.* Hybrid vigor, fetal overgrowth, and viability of mice derived  
744 by nuclear cloning and tetraploid embryo complementation. *Proc. Natl.*  
745 *Acad. Sci. U.S.A.* **98**, 6209–6214 (2001).
- 746 46. Huttlin, E. L. *et al.* A tissue-specific atlas of mouse protein phosphorylation  
747 and expression. *Cell* **143**, 1174–1189 (2010).
- 748 47. Eng, J. K., McCormack, A. L. & Yates, J. R. An approach to correlate  
749 tandem mass spectral data of peptides with amino acid sequences in a  
750 protein database. *J. Am. Soc. Mass Spectrom.* **5**, 976–989 (1994).
- 751 48. Elias, J. E. & Gygi, S. P. Target-decoy search strategy for increased  
752 confidence in large-scale protein identifications by mass spectrometry. *Nat.*  
753 *Methods* **4**, 207–214 (2007).
- 754  
755

## 756 **ACKNOWLEDGEMENTS**

757 We thank members of the Hochedlinger lab for helpful suggestions as well as L.  
758 Barrett for critical reading of the manuscript. Additionally, we thank A. Galvin, M.  
759 Gesner and M. Handley at the Massachusetts General Hospital flow cytometry  
760 core. We also thank A. L. Hawkins, S. Wang, A. Aggarwal and C.C. Morton at  
761 Brigham and Woman’s Hospital CytoGenomics Core Laboratory for karyotyping  
762 analysis. We are grateful to K. Shioda from the Shioda lab for technical support  
763 for genome-sequencing. We are also grateful to W. Yu at The Sidney Kimmel  
764 Cancer Center Microarray Core Facility at Johns Hopkins University for aCGH  
765 analysis, and was supported by NIH grant P30 CA006973 entitled Regional  
766 Oncology Research Center. We thank T. Theunissen and R. Jaenisch for sharing  
767 human OCT4-GFP ESC lines and T. Graf for providing the Rex1-dGFP ESCs.  
768 A.J.H. is supported by an American Cancer Society – New England Division –  
769 Ellison Foundation Postdoctoral Fellowship (PF-15-130-01-DDC). B.D.S. is  
770 supported by an EMBO long-term Fellowship (#ALTF 1143-2015). T. Shioda is  
771 supported by NIH grant (R21ES024861). A.M. is a New York Stem Cell  
772 Foundation Robertson Investigator and supported by NIH grant  
773 (1P50HG006193) and the New York Stem Cell Foundation. K.H. was supported  
774 by funds from the MGH, HHMI, NIH (R01 HD058013-06) and the Gerald and  
775 Darlene Jordan Chair in Regenerative Medicine.

776

## 777 **AUTHOR CONTRIBUTIONS**

778 J.C. and A.J.H. performed bulk of the cell culture, teratomas assays, dot blot and  
779 flow-cytometry analysis; J.C., A.J.H. and S.K. performed the blastocyst  
780 injections; J.C., A.J.H. and J.C. generated the *Mek1/2* DKO iPSC lines; R.M.W.  
781 generated the X<sup>G</sup>X<sup>T</sup> ESC line; J.S. and H.K. generated the *Dnmt* TKO ESC line;

782 J.C., A.J.H. and J.B. conducted the Western blot analysis; J.B., C.M.R. and S.G.  
783 performed the proteomics analysis; B.D.S. performed experiments related to  
784 human ESC culture; J.O. and T.S. performed the genome sequencing analyses  
785 and analyzed the RNA-seq data of interspecies iPSC lines; K.C, H.G. A.M., A.G.  
786 and A.M. performed the RRBS analyses; A.S. and R.I.S. performed the RNA-seq  
787 analyses; K.L. and A.X. conducted the H2A.X ChIP-seq analysis.; J.C., A.J.H.  
788 and K.H. designed the experiments, interpreted the results and wrote the  
789 manuscript.

790

#### 791 **AUTHOR INFORMATION**

792 Reprints and permissions information is available at [www.nature.com/reprints](http://www.nature.com/reprints).  
793 The authors declare no competing financial interests. Readers are welcome to  
794 comment on the online version of the paper. Correspondence and requests for  
795 materials should be addressed to K.H. ([khochedlinger@mgh.harvard.edu](mailto:khochedlinger@mgh.harvard.edu)).  
796

797

798

#### 799 **FIGURE LEGENDS**

800

801 **Figure 1: Erosion of genomic imprints in 2i/L-cultured male ESCs and S/L-**  
802 **cultured female ESCs**

803 (A) Schematic of experimental design. p, passage.

804 (B,C) ICR methylation levels in ESCs at p10 (B) and p20, 23 (C).

805 (D) Allelic expression of the imprinted gene *Impact*.

806 (E,F) Global (D) and ICR (E) methylation levels in male ESCs at p20 and 23 (n=3  
807 biological replicates) and female ESCs at p6 (n=3 biological replicates). ICM,  
808 Inner cell mass.

809 (G) Overlap of differentially methylated regions.

810

811 **Figure 2: Prolonged 2i/L culture impairs the developmental potential of**  
812 **ESCs**

813 (A) Schematic of blastocyst injection protocol.

814 (B) 2n blastocyst injections. Numbers of animals obtained per total number of  
815 transferred embryos are shown. White arrow indicates the protruding tongue of a  
816 female pup. N/D, not determined. Details in Supplementary Table 1.

817 (C) Quantification of coat color chimerism of the chimeras from (B) (top).  
818 Representative images of the varying degrees of chimerism (below).

819 (D) 4n blastocyst injections. Numbers of animals obtained per total number of  
820 transferred embryos are shown. Details in Supplementary Table 2.

821

822 **Figure 3: Impact of prolonged 2i/L culture on chromosomal stability**

823 (A) Karyotyping analysis of male ESC lines. Red boxes indicate abnormal  
824 chromosomes detected.

825 (B-C) Quantification of the chromosomal abnormalities found in 2i/L-cultured (B)  
826 and S/L-cultured (C) male ESCs at p20.

827 (D) Schematic of the  $X^{GX^T}$  ESC line and expected differences between XX and  
828 XO ESCs.

828 (E) Quantification of X chromosome loss in  $X^{GX^T}$  ESCs cultured in S/L or 2i/L.  
829  
830 **Figure 4: Mek1/2 suppression underlies the epigenetic and chromosomal**  
831 **changes observed in ESCs**  
832 (A) Global methylation levels of male ESC cultured in indicated conditions (n=3  
833 biological replicates). White dots, median value.  
834 (B) Global methylation levels of *Mek1/2* double knock-out (DKO) iPSCs and  
835 *GSk3 $\alpha$ / $\beta$*  DKO ESCs cultured in S/L. White dots, median value.  
836 (C) ICR methylation levels in male pluripotent stem cells with the indicated  
837 pharmacological or genetic perturbations.  
838 (D) Differential protein levels between S/L and S/L+PD (>1.5-fold) are plotted  
839 along the y-axis and the corresponding differentially expressed RNAs are plotted  
840 along the x-axis.  
841 (E) Western blot analysis of Dnmt3b and Uhrf1 in the labeled conditions.  
842 (F-G) Global (F) and ICR (G) methylation levels in male ESCs cultured in  
843 indicated conditions. ICM, inner cell mass.  
844 (H) Allelic expression of the imprinted gene *Impact*.  
845 (I) Western blot analysis of Dnmt3b and Uhrf1 in the labeled conditions.  
846 (J) 4n blastocyst injections. Numbers of animals obtained per total number of  
847 transferred embryos are shown. Details in Supplementary Table 2.  
848 (K) Adult all-ESC mice generated using a2i/L-cultured (left) or PKCi/L-cultured  
849 (right) male ESCs.  
850 (L) Chromosomal copy number analysis by whole genome sequencing. Black  
851 arrows indicate trisomies 6 and 8 in 2i/L-cultured ESC lines and the partial  
852 amplification of chromosome 1 in PKCi/L-cultured ESC lines, respectively.  
853 (M) Graphical summary of results.

854  
855

## 856 EXTENDED DATA FIGURE LEGENDS

857

### 858 Extended Data Figure 1: Effect of maintaining the naïve state on DNA 859 methylation in ESCs

860 (a-c) Violin plots showing global methylation levels of ESCs at p10 (a), p20 (b)  
861 and after being placed back into S/L at p23 and 30 (c) by reduced representation  
862 bisulfite sequencing (RRBS). Hypomethylated *Dnmt1* knock-out (KO) ESCs were  
863 included as control. White dots, median value.  
864 (d) Heatmap of DNA methylation levels at SINE elements in ESCs.  
865 (e) Median methylation levels of different genomic elements in the indicated  
866 conditions.  
867 (f) Box plot showing methylation levels of ICRs cultured in each condition.  
868 (g) ICR methylation levels after being re-exposed to S/L for the indicated  
869 passages.  
870 (h) RNA sequencing was performed on a F1 *Mus musculus* x *Mus spretus* stem  
871 cell line cultured in 2i/L for 6 passages. Normalized read counts of mRNA  
872 transcripts expressed from the paternal or maternal alleles are shown based on

873 multiple allele-discriminating SNPs for each gene (6 or more SNPs per gene).  
874 Statistical analysis (two-tail *t*-tests) for allelic biases of the SNPs is shown.

875 (i) Karyotyping results from two female ESC lines cultured in S/L for 10  
876 passages.

877

878 **Extended Data Figure 2: Effects of prolonged 2i/L culture on H2A.X**  
879 **deposition in ESCs**

880 (a) Heatmap showing global H2A.X deposition loss relative to male ESCs  
881 cultured in S/L. Three ESC lines per condition (male S/L, male 2i/L, female S/L)  
882 at passage 10 and two ESC lines (male 2i/L to S/L) at passage 30 were analyzed  
883 (see Fig. 1a).

884 (b) Bar graph quantifying the percentage of H2A.X depleted regions relative to  
885 male ESCs cultured in S/L. Each bar represents median values of biological  
886 replicates of samples in (a).

887 (c) Relative H2A.X deposition on a representative chromosome. Relative losses  
888 (green bars) or gains (gray bars) of H2A.X are mapped to their location on  
889 chromosome 2.

890 (d) Overlap of devoid H2A.X regions common to both female ESCs cultured in  
891 S/L and male cells cultured in 2i/L.

892 (e) H2A.X devoid regions present in the overlap identified in (d) were significantly  
893 enriched for genes involved in the listed developmental pathways. The GREAT  
894 bioinformatic database was used to bin the genes identified into transcriptional  
895 networks.

896

897 **Extended Data Figure 3: Developmental potential of ESCs cultured in S/L**  
898 **and 2i/L.**

899 (a) Representative image of a chimeric pup derived from female ESCs cultured in  
900 S/L (left) compared to a pup obtained through natural mating (right). Body weight  
901 of each pup was shown below.

902 (b) Representative image of a low-grade adult chimera with patches of agouti  
903 hairs generated using female ESCs in S/L (white arrow). Her agouti germline  
904 offspring (red arrowhead) was generated by crossing her to a C57B6 wild-type  
905 mouse.

906 (c) Representative image of all-ESC adult mice generated from male ESCs  
907 cultured in S/L for 10 passages.

908 (d) Bar graphs showing percentages of transferred 4n blastocysts that survived  
909 to birth (“Full-term”), established regular breathing (“Breathing”) or survived past  
910 5 weeks (“Adult”) using male ESCs grown in either S/L (blue bars) or 2i/L (red  
911 bars) until passage 20. The number of animals obtained per total number of  
912 transferred embryos is shown.

913 (e) Representative images of all-ESC neonates produced from male ESCs  
914 cultured in S/L (left) and 2i/L (middle) at passage 20. Representative image of all-  
915 ESC adult mice generated from ESCs cultured in S/L at passage 20 (right).

916

917 **Extended Data Figure 4: Differentiation potential of male ESCs cultured in**  
918 **2i/L.**

919 (a) Karyotype analysis of male ESC lines grown in 2i/L at p10.  
920 (b) Representative images of teratomas produced with three male ESC lines  
921 grown in 2i/L at p20 with depiction of germ layer differentiation where detectable.

922

923 **Extended Data Figure 5: Effects of prolonged 2i/L culture on chromosomal**  
924 **stability in ESCs**

925 (a) Array comparative genomic hybridization (aCGH) analysis of the J-35 ESC  
926 line cultured in S/L or 2i/L condition for the indicated passage numbers.

927 (b) Karyotype analysis of *Rex1-dGFP* ESC line grown in 2i/L for 8 passages after  
928 receiving the line. Red boxes indicate abnormal chromosomes detected.

929 (c) Karyotype analysis of J35 ESC line grown in 2i/L in the absence of a layer of  
930 MEF feeder cells for 16 passages (p20). Red boxes indicate abnormal  
931 chromosomes detected.

932 (d) aCGH analysis on DNA isolated from a newborn pup generated by 4n  
933 blastocyst injection using ESCs cultured in S/L or 2i/L at 20 passages.

934 (e) Combined dendrogram and heatmap depicting ICR methylation levels in  
935 ESCs (n=3 biological replicates) and keratinocytes using RRBS analysis. "2i/L  
936 Keratinocytes" were explanted from chimeric adult mice derived from male 2i/L  
937 ESC p10 and purified by drug selection (G418).

938

939 **Extended Data Figure 6: Characterization of the  $X^G X^T$  ESC line.**

940 (a) Fluorescence microscopic images of  $X^G X^T$  ESCs. GFP/tdTomato double-  
941 positive cells (yellow cells in Merge 1 and 2) indicate two active X chromosomes  
942 while GFP<sup>+</sup>Tomato<sup>-</sup> colony depicts cells that lost one of the X chromosomes.

943 (b) GFP/tdTomato double-positive  $X^G X^T$  ESCs were sorted at passage 5 and  
944 plated in S/L (p6) before measuring the percentage of double-positive and single-  
945 positive cells at p8, 10, 13 and 16 using flow cytometry.

946 (c) Karyotype analysis of undifferentiated,  $X^G O$  (GFP-positive) or  $X^T O$  (tdTomato-  
947 positive) ESCs (left) and GFP/tdTomato double-positive  $X^G X^T$  ESCs (right).  
948 GFP/tdTomato double-positive  $X^G X^T$  ESCs were sorted at passage 5 and  
949 maintained in S/L for 9 passages before analyzed. This result confirms that the  
950 progressive loss of GFP or TdTomato signal was due to the loss of an X and not  
951 X-inactivation due to differentiation.

952

953 **Extended Data Figure 7: Consequences of PD and CHIR treatment on DNA**  
954 **methylation.**

955 (a) Global methylation levels of were analyzed by 5mC dot blot analysis for male  
956 and female ESC lines cultured in the indicated conditions for 6 passages.

957 (b) Median methylation levels at the indicated genetic elements following  
958 inhibition or loss of Mek1/2 or Gsk3 $\alpha/\beta$ , respectively.

959 (c) Violin plots showing global methylation levels of male and female ESCs  
960 cultured in S/L for 6 passages and then cultured for an additional 3 passages in  
961 S/L supplemented with PD. White boxes indicate median methylation levels.

962 (d) Heatmap and dendrogram of ICR methylation levels in male and female  
963 ESCs shown in (c).

964

965 **Extended Data Figure 8: Chromosomal aberrations that occur in 2i/L**  
966 **cultured ESCs are in part due to Mek1/2 inhibition.**

- 967 **(a)** Quantification of relative RNA and protein levels of pluripotency-related genes  
968 between male ESCs in S/L (n=2 technical replicates) and male ESCs in S/L+PD  
969 (n=2 technical replicates).  
970 **(b)** Quantification of relative RNA and protein levels of genes that facilitate DNA  
971 methylation between male ESCs in S/L (n=2 technical replicates) and male  
972 ESCs in S/L+PD (n=2 technical replicates) (see Fig. 4d).  
973 **(c-d)** Karyotype analysis of male ESCs cultured in S/L for 4 passages and  
974 subsequently cultured in either S/L+PD (c) or S/L+CHIR (d) for additional 16  
975 passages. +Mar stands for chromosomal fragment of unknown origin. Red boxes  
976 indicate abnormal chromosomes detected.  
977 **(e)** Western blot analysis of a Dnmt cTKO ESC line for Dnmt1, Dnmt3a and  
978 Dnmt3b after treatment with either 4-OHT or EtOH for one passage.  
979 **(f)** Karyotype analysis of a Dnmt cTKO ESC line that was treated with either 4-  
980 OHT or EtOH for one passage and subsequently cultured for 15 passages in S/L.  
981

982 **Extended Data Figure 9: Characterization of alternative culture conditions**  
983 **for ESCs.**

- 984 **(a)** Representative images of XY ESCs cultured in the indicated conditions.  
985 **(b)** Heatmap and dendrogram of global gene expression levels in male ESCs  
986 cultured in the indicated conditions.  
987 **(c)** Principal component analysis of ESCs cultured in S/L, 2i/L, a2i/L or PKCi/L  
988 using a previously published set of known pluripotency and differentiation  
989 genes<sup>22</sup>. Two male ESC lines maintained in S/L for 4 passages were switched to  
990 each condition and cultured for additional 6 passages (final passage 10).  
991 **(d)** Heatmap and dendrogram showing expression levels of pluripotency and  
992 developmental genes<sup>22</sup> in male ESC lines cultured in the indicated conditions.  
993 **(e)** Relative expression levels of transcripts associated with naïve pluripotency in  
994 (d).  
995 **(f)** Violin plots of global methylation levels in the indicated ESC lines. White dots,  
996 median value.  
997 **(g)** Heatmap and dendrogram of ICR methylation levels in the indicated ESCs  
998 lines.  
999 **(h)** Flow-cytometric analysis of GFP and TdTomato after culturing X<sup>G</sup>X<sup>T</sup> ESCs in  
1000 S/L, S/L+PD and a2i/L for the indicated passages.  
1001 **(i)** Agouti germline offspring (red arrows), obtained from across between an all-  
1002 ESC male generated from p10 a2i/L-cultured ESCs and a C57B6 female.  
1003 **(j-k)** Karyotype analysis of male ESCs cultured in a2i/L for 6 or 16 passages (j),  
1004 or PKCi/L for 6 or 16 passages (k). Red boxes indicate abnormal chromosomes  
1005 detected.  
1006

1007 **Extended Data Figure 10: MEK1/2-independent culture of naïve hESCs**

- 1008 **(a)** Representative image of human ESCs (hESCs) carrying a naïve-specific  
1009 OCT4-EGFP reporter ( $\Delta$ PE-Oct4GFP)<sup>23</sup> cultured in the presence of small

1010 molecule inhibitors of the ROCK, MEK1/2, GSK3 and PKC kinases (t2iLGöY)<sup>24</sup>.  
1011 Bright field image (left) and GFP expression (right).  
1012 **(b)** Representative image of  $\Delta$ PE-Oct4GFP hESCs cultured in the presence of  
1013 small molecule inhibitors of the ROCK, SRC, GSK3 and PKC kinases (a2iLGöY).  
1014 Bright field image (left) and GFP expression (right).  
1015 **(c)** Flow-cytometric analysis of EGFP expression in  $\Delta$ PE-Oct4GFP hESCs  
1016 cultured in t2iLGöY or a2iLGöY.  
1017



**Figure 1.**

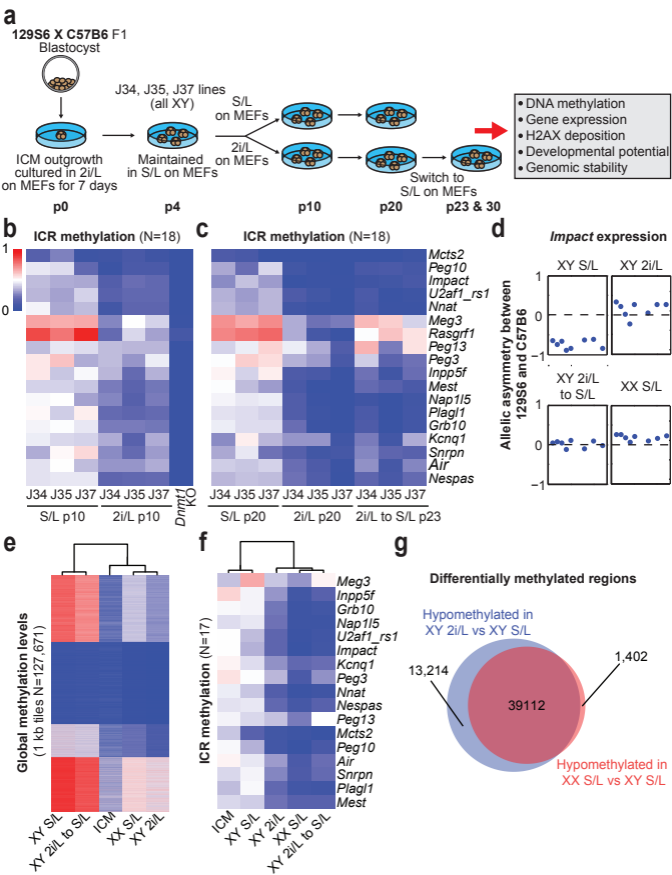


**Figure 2.**

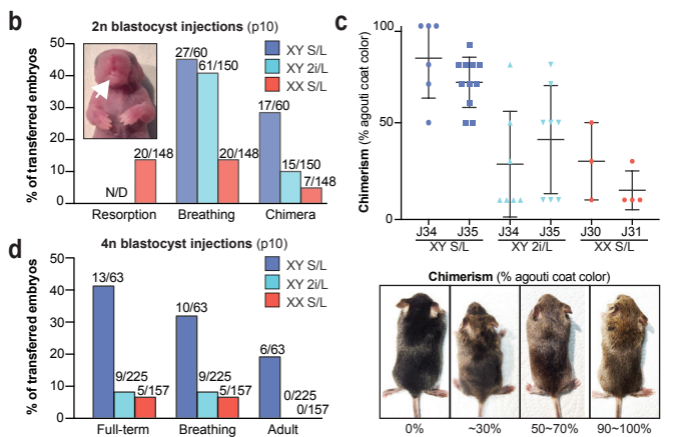
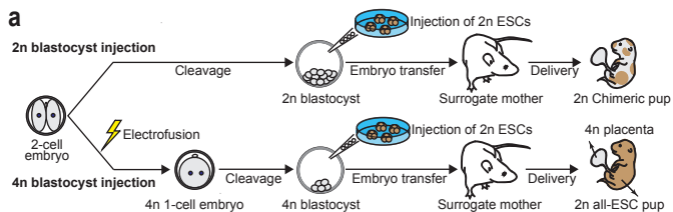
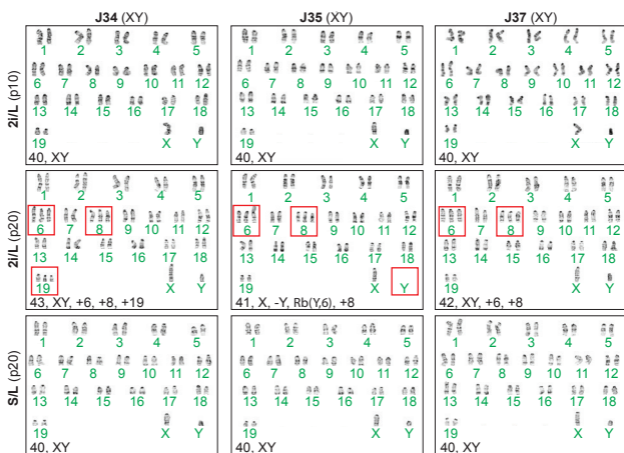
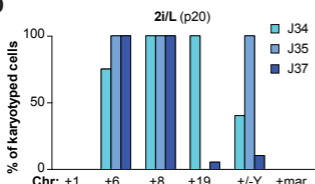


**Figure 3.**

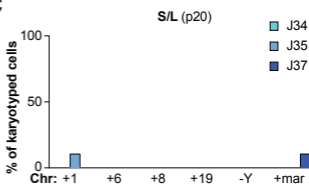
**a**



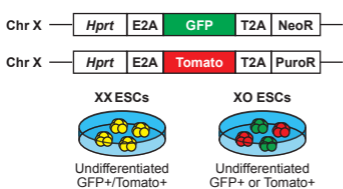
**b**



**c**



**d**



**e**

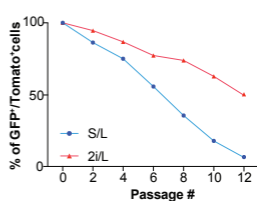


**Figure 4.**

